Journal of Materials Chemistry C

Accepted Manuscript

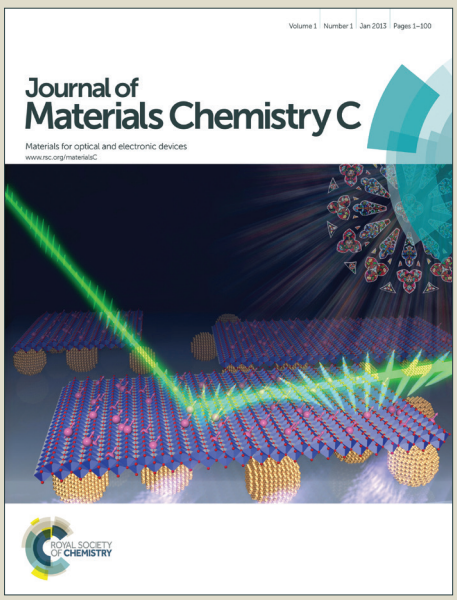

ROYAL SOCIETY OF CHEMISTRY

www.rsc.org/materialsC

Spin Frustration in Antiperovskite Systems: $(TTF^{\bullet+}$ or $TSF^{\bullet+})_3[(Mo_6X_{14})^{2-}Y^-]$

Takaaki Hiramatsu,*[a] Yukihiro Yoshida,[a] Gunzi Saito,*[a,b] Akihiro Otsuka,[c] Hideki Yamochi,[c] Yasuhiro Shimizu,[d] Yuma Hattori,[e] Yuto Nakamura,[e] Hideo Kishida,[e] Hiroshi Ito,[e] Kaplan Kirakci,[f]‡ Stéphane Cordier,[f] and Christiane Perrin[f]

[a] *Faculty of Agriculture*, *Meijo University*, *1-501 Shiogamaguchi*, *Tempaku-ku*, *Nagoya 468-8502*, *Japan*
[b] *Toyota Physical and Chemical Research Institute*, *41-1*, *Yokomichi*, *Nagakute*, *Aichi 480-1192*, *Japan*
[c] *Research Center for Low Temperature and Materials Sciences*, *Kyoto University*, *Sakyo-ku*, *Kyoto 606-8501*, *Japan*
[d] *Department of Physics*, *Graduate School of Science*, *Nagoya University*, *Nagoya 464-8602*, *Japan*
[e] *Department of Applied Physics*, *Nagoya University*, *Chikusa-ku*, *Nagoya 464-8603*, *Japan*
[f] *Institut des Sciences Chimiques de Rennes*, *UMR CNRS 6226*, *Université de Rennes 1, Avenue du Général Leclerc*, *35042 Rennes cedex, France*

Present address ‡ *Institute of Inorganic Chemistry of the Academy of Sciences of the Czech Republic*
Corresponding authors Takaaki Hiramatsu; *E-mail:* htakaaki@meijo-u.ac.jp
Gunzi Saito; *E-mail:* gsaito@meijo-u.ac.jp

Abstract

Two novel antiperovskite charge-transfer (CT) solids composed of a tetraselenafulvalene radical cation ($TSF^{\bullet+}$), dianionic molybdenum cluster unit $[Mo_6X_{14}]^{2-}$, and halogen anion (Y^-) (X, Y = Cl, Br) were prepared by electrocrystallization. Their crystal structures and magnetic properties with regard to spin frustration are discussed together with those of isostructural tetrathiafulvalene (TTF) CT solids previously reported. Both TSF and TTF salts have an apex sharing distorted octahedral spin lattice with a rhombohedral $R\bar{3}$ space group. The calculated overlap integrals based on the crystal structures and insulating nature of the TSF salts indicate that they are Mott insulators. Their spin susceptibilities obeyed the Curie–Weiss law and exhibited an antiferromagnetic ordering at lower temperatures for the TSF salts (Néel temperature, T_N = 3.0 K for X = Y = Cl and 5.5 K for X = Y = Br) than the TTF salts. The Curie–Weiss temperatures ($|\Theta_{CW}|$ ~ 1.6–6.3 K) for the TSF salts are lower than those of the TTF salts. For the TSF salts, spin-flop behavior was detected at 3.2 T for X = Y = Cl and 1.5 T for X = Y = Br at 1.9 K. Due to both the distortion of the octahedral geometry of the spin lattice and the anisotropic molecular orientation, the geometrical spin frustrations in TSF and TTF systems are weakened.

1. Introduction

Geometrical spin frustration suppresses classical long-range magnetic ordering of the Néel state and allows novel quantum states such as the quantum spin liquid (QSL) state to exist in two-dimensional (2D) S = 1/2 antiferromagnets, as proposed by Anderson.[1] Such systems have been theoretically predicted to have a ground state with many degenerate states.[2] To obtain spin-frustrated materials, the geometries of competing spin lattices are crucial. Triangular, kagome, pyrochlore, tetrahedral, octahedral, and

hyperkagome, which is a three-dimensional (3D) version of kagome, spin lattices have previously been discussed (Fig. 1).[3] In some cases, a compromise non-frustrated spin configuration such as a spiral (120°) or collinear order for triangle[4] and 109° for tetrahedron spin lattice,[3b] are discussed.

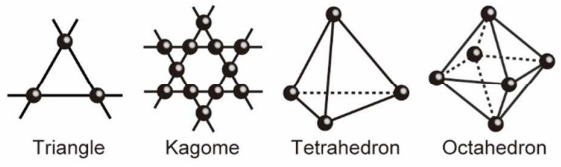

Fig. 1. Geometries of spin lattices having strong spin frustration.

The Curie–Weiss temperature (Θ_{CW}) is a parameter that determines the capability of accessing the QSL state, with the absolute value of Θ_{CW} increasing upon increasing the magnetic exchange interaction $|J|$. J is represented by Eq. 1,

$$J \approx -4t^2/U \quad (1)$$

where t and U are the transfer interaction and effective on-site Coulomb repulsion energy, respectively. The frustration index (f) is defined by Eq. 2, where T_m is the temperature at which magnetic order occurs, was proposed as a measure of spin frustration. When $f > 10$, this is thought to indicate a system with strong spin frustration,[3a,5] while a real QSL system should have $f \sim \infty$.

$$f = -\Theta_{CW}/T_m \quad (2)$$

However, almost no QSL systems have been obtained for materials with a large spin quantum number ($S > 1/2$), even though the geometry of the spin lattice is triangular or kagome with strong spin frustration.[3,6] The first QSL system is a dimer-type Mott insulator κ-$(ET)_2Cu_2(CN)_3$,[7a] which is a charge-transfer (CT) solid between an electron donor ET (Fig. 2a; bis(ethylenedithio)tetrathiafulvalene) and a counteranion $Cu_2(CN)_3^{1-}$. An ET dimer has a +1 charge and a spin value of 1/2. The localized spins on ET dimers of κ-$(ET)_2Cu_2(CN)_3$ form a nearly equilateral triangular lattice in terms of interdimer transfer interactions (t'/t = 1.09, Fig. 2b). The QSL state was confirmed by NMR spectroscopy, spin susceptibility, and μSR measurements down to 20 mK ($|J|/k_B$ = 250 K, $|\Theta_{CW}|$ = 375 K, $f > 1.8\times10^4$).[7a,b,d] Since the discovery of the QSL state in κ-$(ET)_2Cu_2(CN)_3$, several materials based on triangular or kagome lattices were reported to have such a spin state.[8-10] Some examples include $EtMe_3Sb[Pd(dmit)_2]_2$ (triangular spin lattice, dmit: 4,5-dimercapto-1,3-dithiole-2-thione, S = 1/2, $t'/t \sim 0.9$, $|J|/k_B$ = 220–250 K, $|\Theta_{CW}|$ = 325–375 K, $f > 1.6\times10^4$),[11] κ-H_3(Cat-EDT-TTF)$_2$ (triangular spin lattice, H_2(Cat-EDT-TTF): catechol-fused ethylenedithiotetrathiafulvalene, S = 1/2, $t'/t \sim 1.48$, $|J|/k_B$ = 80–100 K, $|\Theta_{CW}|$ = 120–150 K, $f > 2.4\times10^3$),[12] $ZnCu_3(OH)_6Cl_2$ (kagome spin lattice, S = 1/2, $|J|/k_B$ = 197 K, $|\Theta_{CW}| \sim 300$ K, $f > 8.9\times10^3$),[13] and $Na_4Ir_3O_8$ (hyperkagome spin lattice, $|J|/k_B$ = 300 K, S = 1/2, $|\Theta_{CW}|$ = 650 K, $f > 325$).[14] Only the QSL state of κ-$(ET)_2Cu_2(CN)_3$ neighbors to superconducting state among them.[7c,e] Recently we added new candidate κ-$(ET)_2B(CN)_4$ with triangular spin lattice (t'/t = 1.42, S = 1/2) which exhibits quantum critical behavior over a wide temperature range 5–100 K and undergoes a transition to a valence bond crystal ground state below 5 K.[15]

Based on the crystal and band structures and transport properties, we have proposed the following requirements (**A**–**F**) for designing principle of the materials with a QSL state next to a superconducting state for κ-$(ET)_2X$: [**A**] small S value (S = 1/2); [**B**] the system should be a Mott insulator ($W < 0.57$ eV and U/W

> 0.89 at room temperature (RT) for ET systems, where W is the width of upper HOMO band); [**C**] the Mott insulating state has a partial CT state close to the itinerant region; [**D**] the spin lattice should have a geometry which exerts strong geometrical frustration ($t'/t > 0.9$ for triangular spin lattice); [**E**] high $|\Theta_{CW}|$, high $|J|$, and high f values are required to observe the QSL state at the experimentally available temperature; and [**F**] the material must maintain weak energy dispersion along the weakest direction in the case of magnetic interactions of the 2D system.[16]

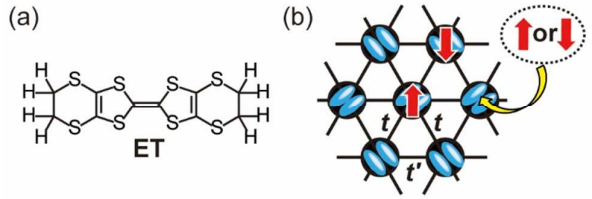

Fig. 2. (a) Chemical structure of ET. (b) Schematic view of the triangular spin lattice of a dimer-type Mott insulator of κ-$(ET)_2X$. Cyan ellipsoids are ET molecules and black circles represent one spin site of the ET dimer. t and t' are interdimer transfer integrals, with t'/t representing the shape of the triangular spin lattice. Red arrows indicate spins.

Since tetragonal and octahedral spin lattices have high potential for geometrical spin frustration, examination of these spin lattices is very important for further development of QSL systems. Thus far, tetragonal and octahedral spin lattices have been very limited in organic solids, whereas several systems are known in inorganic solids. With regard to the tetragonal spin lattice, pyrochlore (e.g., $Na_4I_3O_8$) and B-site spinel (e.g., $ZnCr_2O_4$: $S = 3/2$, $|\Theta_{CW}| = 390$ K, $T_N = 16$ K, $f = 24$) are representative systems, where T_N is the Néel temperature.[3a] For the octahedral spin lattice, octahedral solid $Na_3[Co_6O(OH)(C_8H_4O_4)_6]H_2O$ ($C_8H_4O_4$: isophthalate dianion) is known to have a high $|\Theta_{CW}|$ (118.5 K),[17] whereas cubic antiperovskite manganese Mn_3AX (A: transition metal and semiconductive element, X: C or N) are known to have large negative thermal expansion at the T_N with a peculiar noncollinear magnetic structure.[18] Batail et al. reported that the tetrathiafulvalene (TTF, Fig. 3a) cation radical molecule $TTF^{\bullet+}$ afforded an antiperovskite (octahedral) spin lattice with cluster anions $[Re_6Se_5Cl_9]^{2-}$ [19a] or $[Mo_6X_{14}]^{2-}$ [19b] and a halogen anion (Y^-). In the case of the $[Mo_6X_{14}]^{2-}$ cluster unit, there have been four CT solids formulated as $(TTF^{\bullet+})_3[(Mo_6X_{14})Y]$ (X = Y = Cl; X = Br, Y = Cl, Br, I), where the six molybdenum atoms form an octahedron, eight X atoms occupy the X^i sites (i: inner), and the latter six atoms are positioned in the X^a sites (a: apical) (Figs. 3b, 3c). Although these solids exhibit antiferromagnetic (AF) ordering at 6.2–8.2 K with weak frustration (f = 1.5–2.0), to the best of our knowledge, they are the unique examples of organic octahedral spin lattices. Here, we extended the study of the octahedral spin lattice using tetraselenafulvalene (TSF, Fig. 3a) and obtained $(TSF)_3[(Mo_6Cl_{14})Cl]$ (**1**) and $(TSF)_3[(Mo_6Br_{14})Br]$ (**2**), which were isostructural solids with increased overlap integrals ($\propto t$). We also examined the spin frustration in these crystals based on the above requirements for a QSL system.

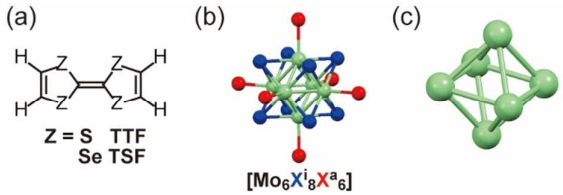

Fig. 3. (a) TTF and TSF molecules. (b) $[Mo_6X^i{}_8X^a{}_6]^{2-}$ cluster unit. Mo: pale green, face-capped inner halogens (X^i): blue, terminal apical halogens (X^a): red. (c) Mo_6 skeleton in a $[Mo_6X^i{}_8X^a{}_6]^{2-}$ cluster unit.

2. Experimental

2.1 Electrocrystallization

Electrooxidation of TSF in the presence of $(TBA)_2[Mo_6X_{14}]$ (TBA: tetrabutylammonium) and TBA•Y (X = Y = Cl, Br, I) afforded antiperovskite compounds $(TSF)_3[(Mo_6X_{14})Y]$ for X = Y = Cl and Br, but not for X = Y = I. Typically, TSF (40 μmol) was added to the anodic compartment, whereas $(TBA)_2[Mo_6X_{14}]$[20] (25 μmol) and TBA•X (25 μmol) were added to the cathodic compartment. After being dissolved in acetonitrile (*ca.* 18 mL), a constant current (1.0 μA) was passed between the two platinum electrodes for approximately one month to afford black, shiny rhombohedral crystals of $(TSF)_3[(Mo_6Cl_{14})Cl]$ (**1**) and $(TSF)_3[(Mo_6Br_{14})Br]$ (**2**) (typically 0.1 × 0.1 × 0.1 mm^3 in size). Other polymorphs with the same space group (rhombohedral $R\bar{3}$) but larger unit cells than those of the antiperovskite systems were also harvested as black crystals for X = Cl, Br, and I; however, only the $[Mo_6X_{14}]$ cluster units were crystallographically refined and the Y content was unknown. In addition, $(TSF)X(H_2O)$ was obtained as a purple crystal for X = Cl. The antiperovskite phases were isolated under a microscope. $(TTF)_3[(Mo_6Br_{14})Br]$ was also prepared according to Ref. 19b.

2.2 Measurements

Single-crystal X-ray diffraction data were collected on a CCD-type diffractometer (Bruker SMART APEX II for 300 K and 100 K and Rigaku Mercury CCD for 25 K) with graphite-monochromated MoKα radiation (λ = 0.71073 Å). The crystal structures were solved by a direct method using SHELXS[21] and refined by a full-matrix least-squares method on F^2 using SHELXL.[21] The crystallographic data and refinement parameters are summarized in Table S1 for **1**, Table S2 for **2**, and Table S3 for $(TTF)_3[(Mo_6Br_{14})Br]$. The CIF files, CCDC 999368 (300 K), 999367 (100 K), and 999366 (25 K) for **1,** 999365 (300 K), 999364 (100 K), and 999363 (25 K) for **2**, 999370 (300 K), and 999369 (100 K) for $(TTF)_3[(Mo_6Br_{14})Br]$, can be obtained free of charge from The Cambridge Crystallographic Data Centre via www.ccdc.cam.ac.uk/data_request/cif.

The direct current conductivity was measured using a standard four-probe technique with platinum wires (ϕ 20 μm) attached to a single crystal with carbon paint (DOTITE XC-12).

A Quantum Design MPMS-XL superconducting quantum interference device (SQUID) magnetometer was used to collect magnetic susceptibility data for polycrystalline samples between 1.9 and 300 K at 0.1–5.0 T. Core diamagnetism values were estimated based on the sum of Pascal's constants (in emu mol^{-1}) for halogen anion Y^- (-0.26×10^{-4} for Cl^- and -0.36×10^{-4} for Br^-) and from the measured value for TSF[22] (-1.27×10^{-4}) and Mo clusters (-2.15×10^{-4} for $[Mo_6Cl_{14}]^{2-}$[23] and -2.62×10^{-4} for $[Mo_6Br_{14}]^{2-}$[24]). ^1H NMR spectroscopic measurements were conducted on polycrystalline samples of **2** in a static magnetic field of 1.51 T between 4.2 and 150 K. The spectra were obtained from Fourier transformation of solid echo $(\pi/2)_{x-\tau}-(\pi/2)_{y-\tau}$ signals. The nuclear spin-lattice relaxation rate (T_1^{-1}) was obtained from the single-exponential nuclear magnetization recovery after the saturation comb pulses between 4.2 and 285 K. Electron paramagnetic resonance (EPR) spectra of a single crystal of **2** were recorded on a JEOL JES-TE200 X band (9 GHz) EPR spectrometer equipped with a JEOL ESCT-470 cryostat from 4.1 to 300 K.

Raman spectra were measured with an inVia Raman microscope (Renishaw) with a He-Ne laser (632.8 nm). UV-Vis-NIR spectra were measured using KBr pellets (3.8–40 × 10^3 cm^{-1}) on a Shimadzu

UV-3100 spectrophotometer. FT-IR spectra were measured using KBr pellets on a Shimadzu Prestige 21 spectrophotometer in the region of 380–7800 cm^{-1}.

2.3 Calculation of transfer integrals

The transfer integrals (t) between TSF (or TTF) molecules were calculated within a tight-binding approximation using the extended Hückel molecular orbital method with single-ζ parameters, including d-orbitals of selenium (or sulfur) atoms based on the crystallographic data.[25] The HOMO of the TSF (or TTF) molecule was used as the basis function. Semi-empirical parameters for Slater-type atomic orbitals were used. The ζ-parameters of atomic orbitals were taken from Ref. 26 for selenium and Ref. 25 for other atoms. The t values were assumed to be proportional to the overlap integral (S) via the equation $t = ES$ (E = −10 eV).

3. Results and Discussion

3.1. Crystal structures and key-keyhole relationship

Salts **1** and **2** are isostructural to the TTF analogs and crystallize in the rhombohedral $R\bar{3}$ space group. Table 1 summarizes the crystallographic data at RT. Figure 4a shows the crystal structure of **2**. Given that the $[Mo_6X_{14}]$ cluster unit has a charge of −2, each TSF molecule is monocationic with S = 1/2. As such, the $[(TSF^{\bullet+})_6Br^-]$ unit depicted in Fig. 4b is the spin lattice unit. When the center of the TSF molecule is indicated by a black circle, six black circles form an octahedral spin lattice based on the point charge approximation. The apex of the octahedron has a positive charge (antiperovskite) contrary to the negative charge in the perovskite system. **1**, **2**, and TTF analogs are approximately represented by the cubic perovskite structure composed of $[(TTF^{\bullet+}$ or $TSF^{\bullet+})_6(Y^-)]$ units, as shown in Fig. 4c, where TTF or TSF are depicted by black balls, Y by orange balls, and $[Mo_6X_{14}]$ clusters by cyan balls. The actual $[(TTF^{\bullet+}$ or $TSF^{\bullet+})_6(Y^-)]$ unit possesses rhombohedral distortion and constructs a 3D framework by sharing vertices. TTF or TSF molecules have short atomic contacts with halogen Y (Fig. S1(a)) or apical halogen X^a in the cluster unit (Fig. S1(b)), as summarized in Table 1.

Table 1 Crystallographic data for $(TTF \text{ or } TSF)_3[(Mo_6X_{14})Y]$ at RT

$D^{\bullet+}$ a)	$[Mo_6X_{14}]^{2-}$ X	Y^-	a/Å	α/°	V/Å^3	Short atomic contact b)/Å with Y	with apical X of Mo_6X_{14}	Edge of octahedron in Fig. 5e (r)/Å r_{blue}	r_{red}	r_{red}/r_{blue}
TSF **1**	Cl	Cl	10.9080(7)	102.3484(3)	1191.8(1)	3.2082(4)	3.2702(9)	6.839	8.498	1.24
TSF **2**	Br	Br	11.1579(5)	101.800(1)	1286.3(1)	3.3252(6)	3.3600(8)	7.037	8.659	1.23
TTF c)	Cl	Cl	10.685(1)	101.54(1)	1134(4)	3.230(2)	3.260(2)	6.758	8.277	1.23
TTF c)	Br	Cl	10.899(1)	100.80(1)	1215(4)	3.312(2)	3.331(2)	6.947	8.398	1.21
TTF d)	Br	Br	10.9429(5)	100.915(1)	1228.5(1)	3.352(2)	3.353(2)	6.967	8.439	1.21
TTF c)	Br	I	11.033(1)	101.35(1)	1251(6)	3.408(2)	3.409(2)	6.992	8.535	1.22

a) D: donor. b) The sum of van der Waals radii: 3.65 Å for Se–Cl, 3.75 Å for Se–Br, 3.55 Å for S–Cl, and 3.65 Å for S–Br.[27] c) Crystallographic data from Ref. 19b. d) Data for newly prepared crystal in our lab, which is in good agreement with the structural analysis in Ref. 19b.

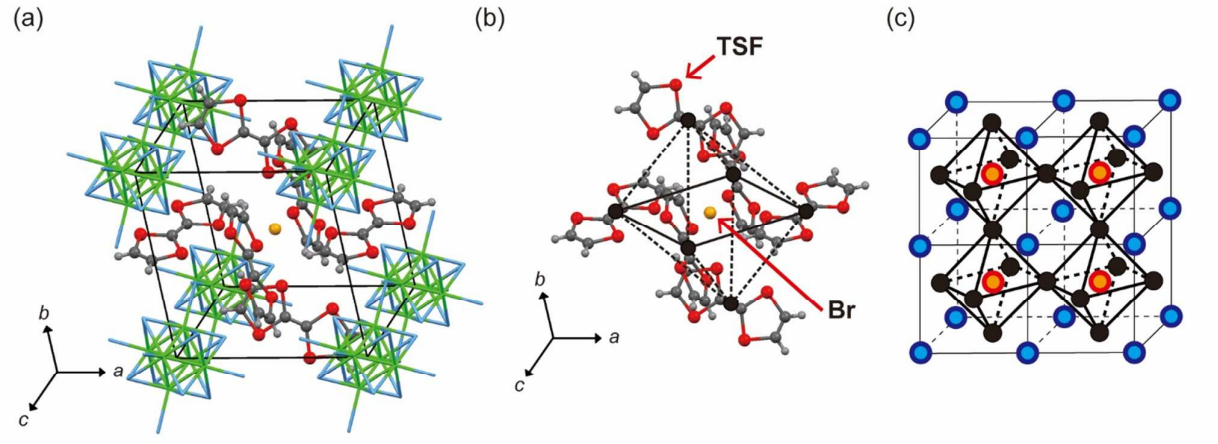

Fig.4. (a) Crystal structure of $(TSF^{\bullet+})_3[(Mo_6Br_{14}^{2-})Br^-]$ (**2**) depicted in ball and stick style. TSF molecules and bromine anion are depicted as balls (gray, dark gray, red, and orange balls are hydrogen, carbon, selenium, and bromine atoms, respectively.) $[Mo_6Br_{14}]$ cluster units are depicted as sticks (green and aqua sticks are molybdenum and bromine atoms, respectively). (b) Unit of octahedral lattice with six TSF molecules and Y = Br. The center of TSF is represented by a black circle. Y = Br (orange) is located at the center of the rectangle represented by solid lines. Octahedral lattice of $(TSF)_6Y$ is made by connecting six black circles (solid and dotted black lines). (c) TSF (or TTF) is represented by black balls, Y by orange balls, and Mo clusters by cyan balls to show a schematic view of the antiperovskite structure.

No structural phase transition was observed in the measured temperature range (300–25 K) for **1** and **2**. Furthermore, Raman spectra of **2** (Fig. S5) in the temperature range from 300–10 K indicate that the charge on the TSF moiety remains unchanged as no significant shift was observed for the charge sensitive bands assigned as $a_g\nu_2$ and $a_g\nu_3$ modes (Fig. S2), with the exception of the change in intensity of overtone and combination bands. The molecular charge of the TSF moiety in **2** is estimated to be +1 by comparing the observed modes with calculated ones of TSF^0 and TSF^{1+} (Fig. S4, Table S4).

We have studied several CT solids of $[Mo_6X_{14}]^{n-}$ and discussed the charge of the donor species based on the Mo–Mo, Mo–X^i, and Mo–X^a interatomic distances in combination with other optical methods.[28] Some of them are presented in Table 2 together with those of $(TBA)_2[Mo_6Cl_{14}]$ and $Cs_2[Mo_6Br_{14}]$.[20] Since the molecular structure of neutral and −1 charge species of $[Mo_6X_{14}]^{n-}$ are not available, the charge estimated by the bond lengths of $[Mo_6X_{14}]^{2-}$ may not be completely accurate. However, the observed distances show excellent consistency with the −2 charge of $[Mo_6X_{14}]^{n-}$. The Raman spectral results as well as the assignment of the charge of Mo cluster units support the +1 charge of the TSF moiety (S = 1/2), which is consistent with the SQUID and EPR data (*vide infra*); satisfying requirement [**A**] for a QSL system.

Table 2. Average Mo–Mo, Mo–X^i, and Mo–X^a interatomic distances (Å)

Salt of $[Mo_6X_{14}]$ cluster unit		Mo–Mo	Mo–X^i	Mo–X^a	Charge on $[Mo_6X_{14}]$	Ref.
$Cs_2[Mo_6Br_{14}]$		2.635	2.601	2.600	−2	20a
$(TBA)_2[Mo_6Cl_{14}]$		2.602	2.469	2.420	−2	20b
Donor of CT solid[a)]	X					
TTT	Br	2.635	2.606	2.594	−2	28a
BO	Br	2.630	2.604	2.594	−2	28a
Perylene	Br	2.637	2.604	2.586	−2	28a
Coronene	Cl	2.607	2.478	2.426	−2	28b
Coronene	Br	2.633	2.599	2.592	−2	28b
TSF **1**	Cl	2.608	2.476	2.430	−2	This work
TSF **2**	Br	2.635	2.602	2.594	−2	This work
$(TTF)_3[(Mo_6Br_{14})Br]$		2.635	2.603	2.594	−2	This work

a) TTT: tetrathionaphthacene, BO: bis(ethylenedioxy)-TTF.

Figure 5 shows the relationship between the spin site (key) and the architecture (keyhole), which holds the key part for (TTF or TSF)$_3$[(Mo$_6$X$_{14}$)Y]. The keyhole is the lattice formed by the [Mo$_6$X$_{14}$]$^{2-}$ cluster units (Figs. 5a and 5a′), whereas the key is the octahedral spin lattice unit of [(TTF or TSF)$_6$Y] (Figs. 5b and 5b′). The cluster units form a pseudocubic arrangement, in which each corner is occupied by a cluster and the spin site [(TTF or TSF)$_6$Y] fits into the center of the cube. Such key(spin-site)–keyhole(architecture) consideration would provide a clue to develop new spin-frustrated system. The (TTF or TSF)$_3$[(Mo$_6$X$_{14}$)Y] crystal is assembled by nesting the key into the keyhole equivalent to the unit cell through short atomic contacts and Coulomb interactions (Figs. 5c and c′). However, the actual structure of the rhombohedral unit cell ($\alpha \sim 101$–$102°$, Table 1) is a distorted octahedron (Fig. 5d), resulting in two different distances between the centers of TTF (or TSF) molecules, as depicted in blue and red in Fig. 5e and summarized in Table 1. It is noticeable that the ratios of the distances in blue and red (r_{red}/r_{blue}) are nearly identical among the (TTF or TSF)$_3$[(Mo$_6$X$_{14}$)Y] salts, as shown in Table 1, since r_{red}/r_{blue} is proportional to angle α ($r_{red}/r_{blue} = 1$ at $\alpha = 90°$). The difference in the distances and relative orientation between two TTF (or TSF) molecules gives rise to two different overlap integrals, $s1$ and $s2$ (*vide infra*). This indicates that the (TTF or TSF)$_3$[(Mo$_6$X$_{14}$)Y] salts roughly satisfy requirement [**D**], but not in the strict sense. The strictness of requirement [**D**] for a QSL system is discussed in Section 3.3.

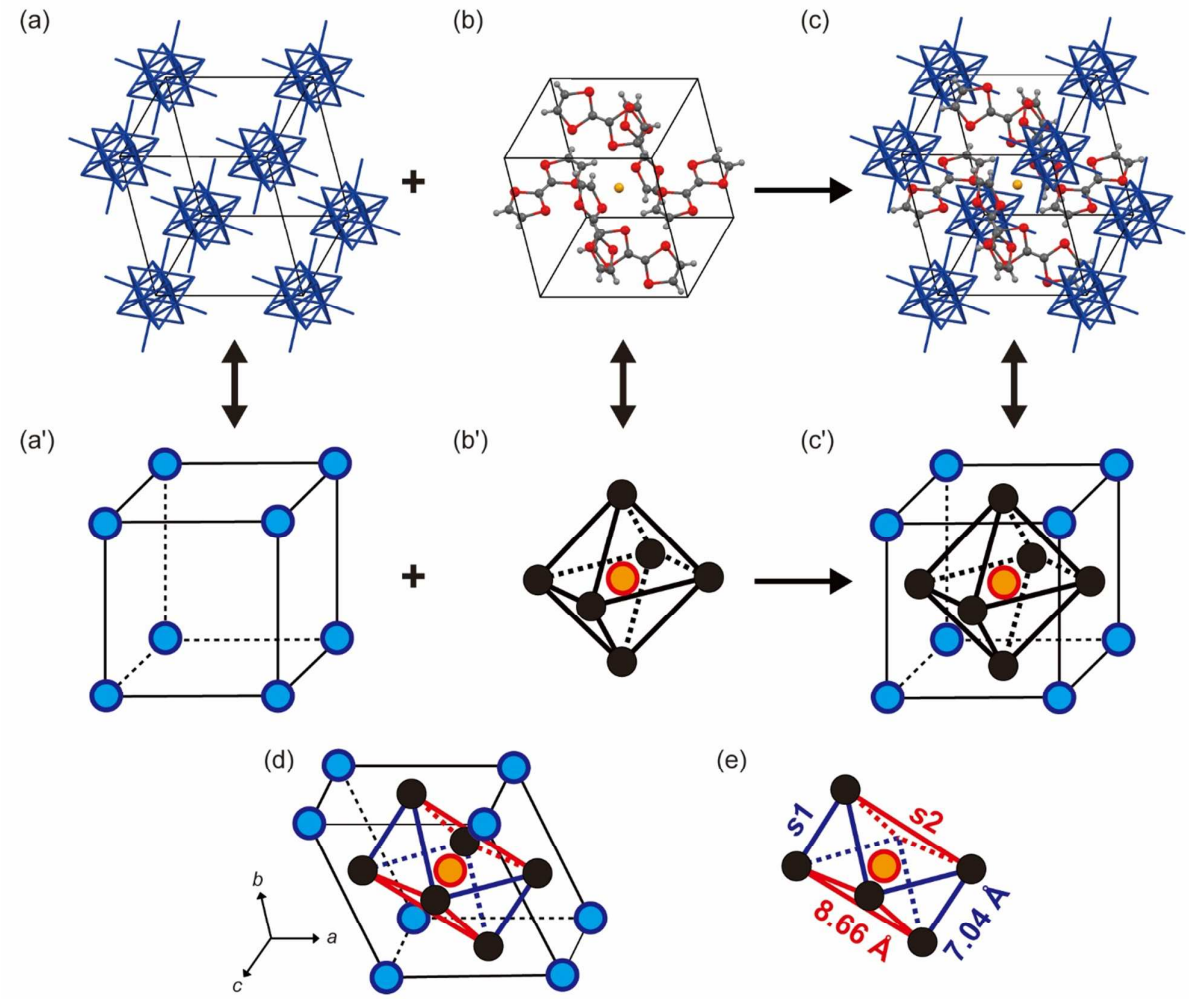

Fig. 5. Key–keyhole relationship of (TTF or TSF)$_3$[(Mo$_6$X$_{14}$)Y]. (a, a′) The lattice formed by [Mo$_6$X$_{14}$]$^{2-}$ cluster units. (b, b′) The lattice composed of TTF$^{\bullet+}$ (or TSF$^{\bullet+}$) and Y$^-$. (c, c′) Unit cell of (TTF or TSF)$_3$[(Mo$_6$X$_{14}$)Y]. (d) Rhombohedral packing of (TTF or TSF)$_3$[(Mo$_6$X$_{14}$)Y]. Blue circles: [Mo$_6$X$_{14}$]$^{2-}$ cluster units. Orange circle: Y$^-$. Black circles: TTF$^{\bullet+}$ or TSF$^{\bullet+}$. (e) Overlap integrals s1(blue) and s2(red) between TTF (or TSF) molecules in (TTF or TSF)$_3$[(Mo$_6$X$_{14}$)Y]. The intersite distances are those of (TSF)$_3$[(Mo$_6$Br$_{14}$)Br].

3.2. Transport and magnetic properties

Both TSF salts **1** and **2** are semiconducting with RT resistivities (ρ_{RT}) of 3 × 10^4 Ωcm (activation energy (ε_a) = 0.12 eV) and 2 × 10^4 Ωcm (ε_a = 0.08 eV), respectively (Fig. S6). The temperature dependence of static magnetic susceptibility (χ), χ behavior in various magnetic fields, and magnetic field dependence of dM/dH of **2** are shown in Fig. 6, with **1** exhibiting similar behavior (Fig. S7). The χ at RT (χ_{RT}) is 1.23 × 10^{-3} emu spin^{-1} for **1** and 1.12 × 10^{-3} emu spin^{-1} for **2**, both of which are larger than that of (TTF)$_3$[(Mo$_6$Br$_{14}$)Br] (1.06 × 10^{-3} emu spin^{-1}) (Fig. S8(a)). These χ_{RT} values are the same as those of typical ET Mott insulators, where χ_{RT} is 9–12 × 10^{-4} emu mol^{-1}.[16] From RT to 20 K, these values obey the Curie–Weiss law with a Curie constant (C) of 0.370 emu K spin^{-1} and Θ_{CW} of −1.6 K for **1** and C = 0.342 emu K spin^{-1} and Θ_{CW} = −6.3 K for **2**, indicating considerably weaker AF interactions than those in TTF salts[19]

(Θ_{CW}: −14.6 ~ −11.5 K). In the lowest temperature region, χ undergoes a sharp decrease at 3.0 K for **1** and 5.5 K for **2**, as seen in Figs. 6(a) and S7(a), which could be suppressed by applying a magnetic field (insets of Figs. 6(a) and S7(a)). This confirms that the ground state of these solids are the Néel state and the occurrence of the spin-flop transition at high magnetic fields. The T_N is lower than those observed for TTF analogs (Table 3). For the spin-flop field (H_{sf}), Fig. 6b clearly shows a peak corresponding to the H_{sf} at 1.5 T (3.2 T for **1** in Fig. S7(b)). Although H_{sf} was not explicitly determined, $(TTF)_3[(Mo_6Br_{14})Br]$ also exhibits the spin-flop phenomenon between 0.1 and 0.2 T at 1.9 K (Figs. S8(a) and (b)). Table 3 summarizes the transport and magnetic properties of $(TTF \text{ or } TSF)_3[(Mo_6X_{14})Y]$. These results, together with the structural analyses and estimated charge on the TSF species, confirm that these salts are Mott insulators and satisfy requirement [**B**] for a QSL system.

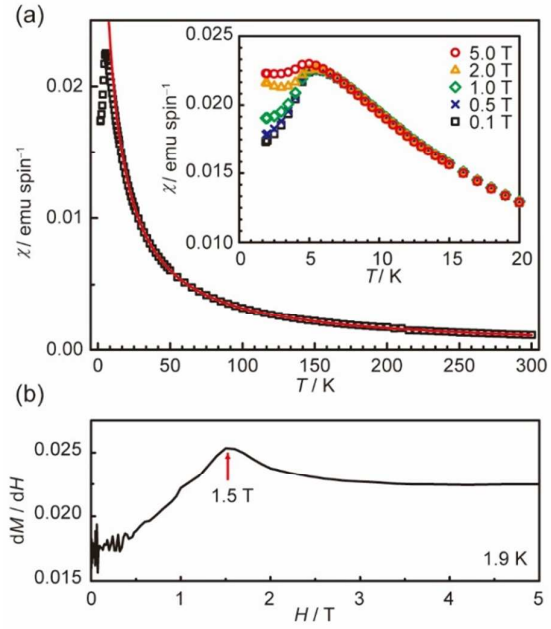

Fig. 6. (a) Temperature dependence of static magnetic susceptibility of polycrystalline **2** at 0.1 T. Solid red line is the Curie–Weiss fit with $C = 0.342$ emu K spin^{-1} and $\Theta_{CW} = -6.3$ K. Inset shows the magnetic field dependence (0.1–5.0 T) of χ below 20 K. (b) dM/dH as a function of magnetic field at 1.9 K. A scatter of dM_p/dH at the region of H = 0.1–0.45 T resulted from inherent properties of the superconducting magnet. A red arrow indicates the spin-flop magnetic field.

Table 3 Transport and magnetic properties and calculated overlap integrals of $(TTF \text{ or } TSF)_3[(Mo_6X_{14})Y]$

$D^{\bullet+}$	X in $[Mo_6X_{14}]^{2-}$	Y^-	Θ_{CW} / K	T_{max} [a] /K	T_N [b] / K	Ref.	f	χ_{RT} /emu mol^{-1}	H_{sf}/T	ρ_{RT} /Ωcm	$s1$ /10^{-3}	$s2$ /10^{-4}	$\lvert s2\rvert/\lvert s1\rvert$	Ref.
TSF	**1** Cl	Cl	−1.6	3.0	3.0	This work	0.53	1.23×10^{-3}	3.2	3×10^4	3.61	7.01	0.20	This work
	2 Br	Br	−6.3	5.5	5.5	This work	1.15	1.12×10^{-3}	1.5	2×10^4	3.48	3.56	0.10	This work
TTF	Cl	Cl	−14.6	11	8.2	19b	1.78	–	–	–	1.12	−0.93	0.08	This work
	Br	Cl	−16.7	13	8.2	19b	2.04	–	–	–	1.10	−1.75	0.16	This work
	Br	Br	−11.5	11	7.5	19b	1.53	1.06×10^{-3}	0.1~0.2	–	1.05	−1.21	0.11	This work
	Br	I	−12.1	8	6.2	19b	1.95	–	–	–	0.86	−0.76	0.09	This work

a) T_{max}: peak temperature of χ in SQUID measurement. b) T_N was evaluated by EPR measurement in ref. 19. For **1** and **2**, T_{max} was used as T_N, as T_N could not evaluated by EPR measurement.

Figure 7 presents the EPR data of **2**. The *g*-factor at RT was 2.0301, which is in agreement with the $TSF^{\bullet+}$ species ($S = 1/2$) ($g_{AV} = 2.027$).[29] The EPR linewidth (ΔH) and *g*-factor show an increase below *ca*. 45 K that may be ascribed to the low-dimensional fluctuation of AF ordering. Below 5 K, both EPR parameters increase rapidly, owing to the 3D AF ordering.

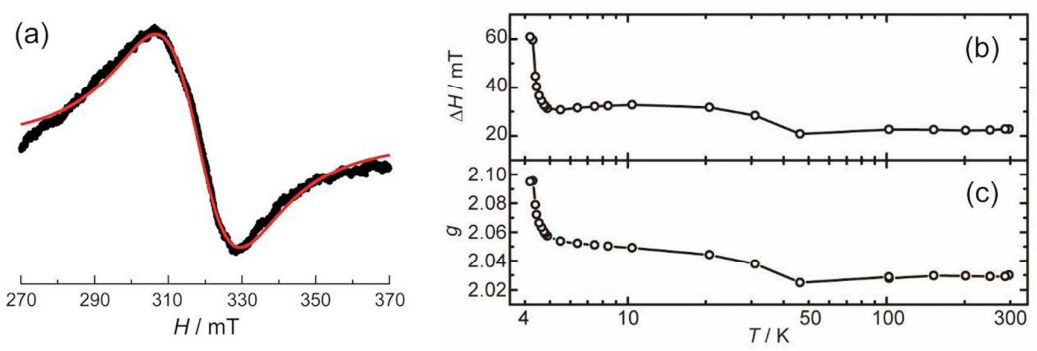

Fig. 7. (a) EPR spectrum of a single crystal of **2** at RT, where a red line shows a single Lorentzian line centered at $g = 2.0301$. Temperature dependence of (b) EPR linewidth (ΔH) and (c) *g*-value.

To give microscopic insight into the ground state, the ^{1}H NMR spectrum was measured for a randomly orientated polycrystalline sample of **2**. The temperature dependence of the ^{1}H NMR spectra in Fig. 8a shows broadening and splitting upon cooling, as indicated by blue and red arrows for the higher and lower frequency peaks, respectively. At high temperatures, the spectral shape is dominated by ^{1}H–^{1}H nuclear dipole coupling. As the spin susceptibility increases, anisotropic hyperfine and dipole fields from electron spins become visible at the ^{1}H sites, giving an anisotropic powder pattern to the NMR spectra. In Fig. 8b, we plot the Knight shifts defined as peak frequencies measured from the central frequency at high temperatures. The Knight shift for a low-frequency peak well correlates to the spin susceptibility as an implicit function of temperature, as shown in Fig. 8c, which yields a hyperfine coupling constant of −0.15 kOe μ_B^{-1}. The Knight shift for a high-frequency peak behaves nearly independent of temperature because of the vanishing hyperfine coupling. A prominent spectral broadening occurs below 5 K, clearly indicating the magnetic order. Using the hyperfine coupling, the observed local field of 1 MHz at 4.2 K corresponds to a magnetic moment of 1.1μ_B, as shown in Fig. 8d. The ^{1}H NMR spin-lattice relaxation rate (T_1^{-1}) shows a divergent peak around 5 K, indicating the 3D nature of the AF transition (Fig. 8e).

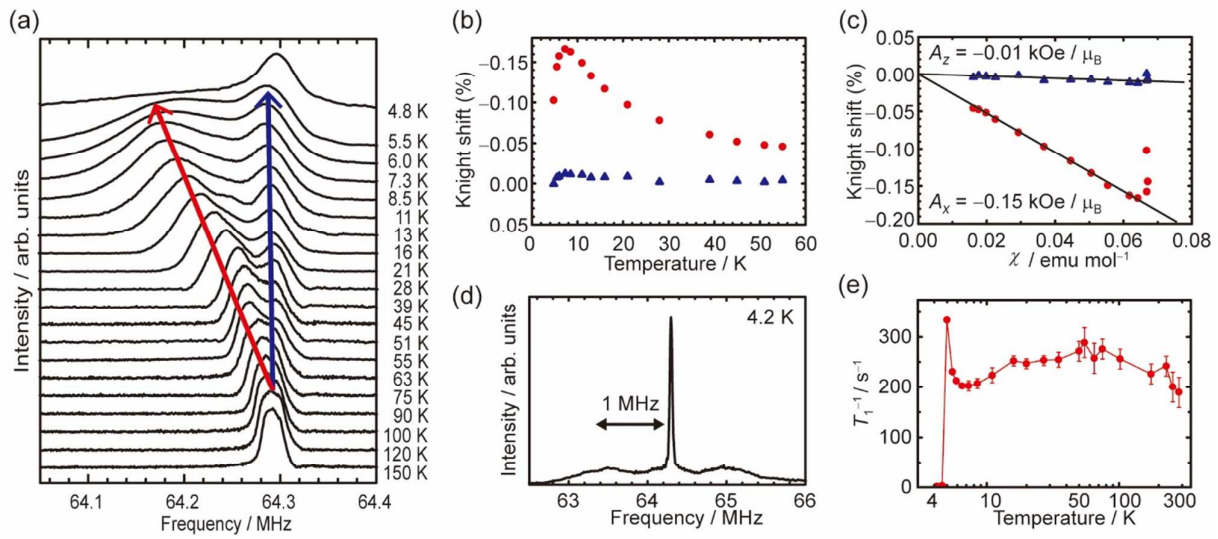

Fig. 8. ^{1}H NMR spectra of polycrystalline **2**. Temperature dependence of (a) ^{1}H NMR spectra; high- and low-frequency peaks are indicated by blue and red arrows, respectively. (b) Temperature dependence of Knight shift. (c) The Knight shifts vs. magnetic susceptibility, where the linearity gives the principal components of the hyperfine coupling, $A_z = -0.01$ and $A_x = -0.15$ kOe μ_B^{-1}. In (b) and (c), blue and red symbols correspond to the blue and red arrows in (a), respectively. (d) The spectrum in the magnetically ordered state at 4.2 K. The sharp central peak comes from the H sites with negligible hyperfine coupling constants. (e) Temperature dependence of nuclear spin-lattice relaxation rate (T_1^{-1}).

3.3. Geometry of spin lattice and spin frustration

Table 3 also summarizes the overlap integrals of (TTF or TSF)$_3$[(Mo$_6$X$_{14}$)Y]. The absolute $s1$ values for the TSF salts (3.5–3.6 × 10^{-3}) lie within those of interdimer overlap integrals observed for the κ-(ET)$_2$X salts (2.9–11.5 × 10^{-3}), which cover Mott insulators, AFs, QSLs, metals, and superconductors.[30] Consequently, as long as $s1$ concerns, the TSF salts may reside near the Mott boundary if the U values are comparable to those of dimer-type conductors, κ-(ET)$_2$X (U_d = 0.45–0.51 eV [16] by extended Hückel method, where U_d is the Coulomb repulsive energy between two electrons on a dimer). However, monomer-type systems such as the present salts have much larger U values than U_d for κ-(ET)$_2$X, as two electrons are present on one molecule.

In the monomer-type systems, the U value is approximated as ($U_0 - V$), where U_0 is bare on-site Coulomb repulsion and V is neighboring-site Coulomb repulsion (Fig. 9). We estimated the U values of **1**, **2**, and (TTF)$_3$[(Mo$_6$Br$_{14}$)Br] through observation of the first CT absorption band peak.[31] The present salts do not possess such regular segregated columns as depicted in Fig. 9, and the distance between neighboring sites is larger compared to the conventional 1D segregated column. Hence, the absorption band originating from U for these salts is not well separated from the higher energy bands and appeared as a shoulder (Fig. S9). The U values derived from the absorption peaks were estimated as 1.2–1.4 eV for **1** and **2** and 1.4–1.5 eV for (TTF)$_3$[(Mo$_6$Br$_{14}$)Br]. Accordingly, the transfer interactions derived from overlap integral $s1$ are much smaller compared to the effective U value for (TSF)$_3$[(Mo$_6$X$_{14}$)Y], indicating that the localized spin nature is in good accordance with the transport results. The $s1$ values of TTF salts are about three times smaller (0.86–1.1 × 10^{-3}) than those of TSF salts, suggesting a more localized nature of the TTF salts.

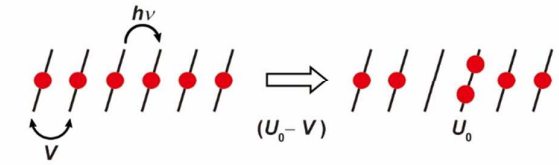

Fig. 9. One-electron transfer in a Mott insulator (thick bars and red balls represent molecules and radical electrons, respectively) costs energy of effective U (= $U_0 - V$) approximately. Such electron transfer is observed as the first absorption band in optical measurements of fully ionized radical CT salts.

The edges drawn by blue lines ($s1$) in Fig. 5e possess one order of magnitude larger overlap integrals than the red lines ($s2$) of the octahedron ($|s1| > |s2|$), mainly owing to the shorter distance (7.04 Å for $s1$ vs. 8.66 Å for $s2$ in **2**). Furthermore, the anisotropic molecular orbital of organic molecules causes a larger difference in $s1$ and $s2$ by forming different relative orientations between two TTF (or TSF) molecules (Fig. 10a for $s1$ and Fig. 10b for $s2$). The very small $s2$ values for both antiperovskite systems (3.6–7.0 × 10^{-4} for TSF salts and 0.76–1.8 × 10^{-4} for TTF salts) cause them to be 3D Mott insulators.

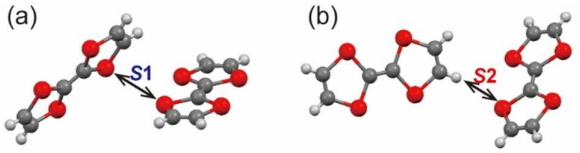

Fig. 10. Relative orientations of two TTF (or TSF) molecules for overlap integrals (a) $s1$ and (b) $s2$.

Table 3 includes the ratio $|s2|/|s1|$, which corresponds to t'/t in the case of a 2D isosceles triangle lattice, a parameter for the spin frustration concerning the triangle composed of two blue edges and one red edge. The ratio $|s2|/|s1|$ is much smaller than unity, indicating that the spin frustration is not significant.

Since the spin frustration is enhanced when $|s2|/|s1|$ approaches unity, it may be reasonable that the T_N values of TSF salts (3.0 K for **1**, 5.5 K for **2**) are lower than those observed for TTF salts in accordance with increased $|s2|/|s1|$. The increase of $|s2|/|s1|$ to unity is favorable for the QSL state; however, upon decreasing temperature, the $|s2|/|s1|$ values decrease to 0.18 and 0.10 at 100 K and 0.17 and 0.09 at 25 K for **1** and **2**, respectively.

The antiperovskite system (TTF or TSF)$_3$[(Mo_6X_{14})Y] was found to have weak spin frustration in terms of f (Table 3). Since the J value is represented by Eq. 1 and U of the TSF molecule is smaller than that of the TTF molecule, the $|\Theta_{CW}|$ values of the TSF salts are thought to be larger than those of the TTF salts. However, the experimental results are the opposite of this expectation in that the $|\Theta_{CW}|$ values of the TSF salts are smaller than those of the TTF salts, even though the absolute values of $s1$ and $s2$ are three times larger than those of TTF salts. The reason for this discrepancy is currently unknown. The AF interactions represented by Θ_{CW} are very weak in this antiperovskite system, compared with the QSL systems: $|\Theta_{CW}|$ = 300, 325–375, 375, and 650 K for $ZnCu_3(OH)_6Cl_2$, $EtMe_3Sb[Pd(dmit)_2]_2$, κ-$(ET)_2Cu_2(CN)_3$, and $Na_4Ir_3O_8$, respectively.[7,11,13,14] As such, the distorted octahedral spin lattice of (TTF or TSF)$_3$[(Mo_6X_{14})Y] is not a QSL system candidate.

Although the antiperovskite salts (TTF or TSF)$_3$[(Mo_6X_{14})Y] satisfy requirements [**A**] and [**B**] for a QSL system, they do not satisfy requirements [**D**] and [**E**], ruling out the possibility of a QSL state and

allowing for the AF Néel state with low $|\Theta_{CW}|$ and T_N. Thus, an undistorted octahedral $[(donor^{\bullet+})_6Y^-]$ unit composed of donor molecules having small effective U values with equal and large overlap integrals between spin sites will be envisaged.

4. Conclusion

TSF molecules afforded antiperovskite salts, $(TSF)_3[(Mo_6X_{14})Y]$ (X = Y = Cl: **1** and X = Y = Br: **2**), isostructural to the TTF analogs. Their crystal structures are interpreted by a key–keyhole relationship between distorted octahedral spin sites [(TTF or TSF)$_6$Y] and the rhombohedral lattice, the corners of which are occupied by cluster anions $[Mo_6X_{14}]^{n-}$. The bond lengths of $[Mo_6X_{14}]^{n-}$ determined by structural analysis suggest that it is in a dianionic state, $[Mo_6X_{14}]^{2-}$, which results in a +1 charge of the TSF species (S = 1/2). This valence of TSF was confirmed by Raman and EPR measurements. The crystal structure and semiconductive nature indicate that they are 3D Mott insulators at RT. A 3D AF ordering occurs and the T_N temperatures for the TSF solids (T_N = 3.0 K for **1** and 5.5 K for **2**) are lower than those for the TTF solids, owing to higher spin frustration in terms of $|s2|/|s1|$. Spin-flop was detected for TSF salts at 3.2 T for **1** and 1.5 T for **2** at 1.9 K. Such spin-flop was also detected for $(TTF)_3[(Mo_6Br_{14})Br]$ at 0.1–0.2 T at 1.9 K. Although the salts satisfy requirements [**A**] and [**B**] for a QSL system, they do not satisfy requirements [**D**] and [**E**]. Owing to both the distortion of the octahedral geometry of the spin lattice and the anisotropic molecular orientation, the geometrical spin frustration in both TSF and TTF systems is weakened. In order to have strong geometrical spin frustration toward the QSL state, $|s1|\sim|s2|$ and larger s values are essential.

Acknowledgments.

The work was supported by JSPS KAKENHI Grants (23225005 and 26288035). Thanks are due to the Instrument Center, the Institute for Molecular Science, for assistance in obtaining the single crystal diffraction data at 25 K.

References

1. a) P. W. Anderson, *Mater. Res. Bull.*, 1973, **8**, 153-160.
   b) P. Fazekas, P. W. Anderson, *Philos. Mag.*, 1974, **30**, 423-440.
2. G. H. Wannier, *Phys. Rev*. 1950, **79**, 357-364.
3. a) A. P. Ramirez, *Annul. Rev. Mater. Sci.*, 1994, **24**, 453-480.
   b) J. E. Greedan, *J. Mater. Chem*., 2001, **11**, 37-53.
4. a) D. A. Huse, V. Elser, *Phys. Rev. Lett.*, 1988, **60**, 2531-2534.
   b) L. F. Tocchio, C. Gros, R. Valenti, F. Becca, *Phys. Rev. B*, 2014, **89**, 235107/1-9.
   c) A. Yamada, *Phys. Rev. B*, 2014, **89**, 195108/1-9.
5. P. Schiffer, A. P. Ramirez, *Comments Condens. Matter Phys*., 1996, **18**, 21-50.
6. a) K. Hirakawa, H. Kadowaki, K. Ubukoshi, *J. Phys. Soc. Jpn.*, 1983, **52**, 1814-1824.
   b) J. L. Manson, E. Ressouche, J. S. Miller, *Inorg. Chem.*, 2000, **39**, 1135-1141.
7. a) Y. Shimizu, K. Miyagawa, K. Kanoda, M. Maesato, G. Saito, *Phys. Rev. Lett.,* 2003, **91**, 107001/1-4.
   b) S. Ohira, Y. Shimizu, K. Kanoda, G. Saito, *J. Low Temp. Phys*., 2006, **142**, 153-158.
   c) Y. Shimizu, H. Kasahara, T. Furuta, K. Miyagawa, K. Kanoda, M. Maesato, G. Saito, *Phys. Rev. B*, 2010, **81**, 224508/1-4.
   d) F. L. Pratt, P. J. Baker, S. J. Blundell, T. Lancaster, S. Ohira-Kawamura, C. Baines, Y. Shimizu, K. Kanoda, I. Watanabe, G. Saito, *Nature*, 2011, **471**, 612-616.
   e) Y. Shimizu, M. Maesato, G. Saito, *J. Phys. Soc. Jpn.*, 2011, **80**, 074702/1-7.
8. L. Balents, *Nature,* 2010, **464**, 199-208.
9. M. R. Norman, *Science*, 2011, **332**, 196-200.

10. B. J. Powell, R. H. McKenzie, *Rep. Prog. Phys*.2011, **74**, 056501/1-60.
11. T. Itou, A. Oyamada, S. Maegawa, M. Tamura, R. Kato, *J. Phys.: Condens. Matter,* 2007, **19**, 145247/ 1-5.
12. T. Isono, H. Kamo, A. Ueda, K. Takahashi, M. Kimata, H. Tajima, S.Tsuchiya, T. Terashima, S. Uji, H. Mori, *Phys. Rev. Lett.*, 2014, **112**, 177201/1-5.
13. a) T.-H. Han, J. S. Helton, S. Chu, D. G. Nocera, J. A. Rodriguez-Rivera, C. Broholm, Y. S. Lee, *Nature*, 2012, **492**, 406-410.
    b) J. S. Helton, K. Matan, M. P. Shores, E. A. Nytko, B. M. Bartlett, Y. Yoshida, Y. Takano, A. Suslov, Y. Qiu, J.-H. Chung, D. G. Nocera, Y. S. Lee, *Phys*. *Rev*. *Lett*., 2007, **98**, 107204/1-4.
14. a) Y. Okamoto, M. Nohara, H. Aruga-Katori, H. Takagi, *Phys. Rev. Lett*., 2007, **99**, 137207/1-4.
    b) R. R. P. Singh, J. Oitmaa, *Phys. Rev. B*, 2012, **85**, 104406/1-4.
15. Y. Yoshida, H. Ito, M. Maesato, Y. Shimizu, H. Hayama, T. Hiramatsu, Y. Nakamura, H. Kishida, T. Koretsune, C. Hotta, G. Saito, *Nat. Phys*., 2015, **11**, 679-683.
16. T. Hiramatsu, Y. Yoshida, G. Saito, A. Otsuka, H. Yamochi, M. Maesato, Y. Shimizu, H. Ito, H. Kishida, *J. Mater. Chem. C*, 2015, 1378-1388. Even though the following solid is reported as a QSL candidate with $S = 1$ ($Ba_3NiSb_2O_9$, J. G. Cheng, G. Li, L. Balicas, J. S. Zhou, J. B. Goodenough, C. Xu, H. D. Zhou, *Phys, Rev. Lett.*, 2011, **107**, 197204/1-4), considering its small $|\Theta_{CW}|$ (= 75.6 K), and f (> 216) values, the solid should be studied down to much lower temperatures in order to confirm its QSL state.
17. C. Livage, N. Guillou, J. Chaigneau, P. Rabu, M. Drillon, G. Ferey, *Angew. Chem. Int. Ed*. 2005, **44**, 6488-6491.
18. K. Takenaka, *Sci*. *Technol*. *Adv*. *Mater*. 2012, **13** 013001/1-11.
19. a) P. Batail, L. Ouahab, A. Penicaud, C. Lenoir, A. Perrin, *C. R. Acad. Sc. Paris, série II*, 1987, **304 nº18**, 1111-1116. It was shown later that the actual compound contained a mixture of monoanionic and dianionic cluster units (see ref. 19b).
    b) P. Batail, C. Livage, S. S. P. Parkin, C. Coulon, J. D. Martin, E. Canadell, *Angew. Chem. Int. Ed.*, 1991, **30**, 1498-1500.
20. a) K. Kirakci, S. Cordier, C. Perrin, *Z. Anorg. Allg. Chem.* 2005, **631**, 411-416.
    b) W. Preetz, K. Harder, H. G. von Schnering, G. Kliche, K. Peters, *J. Alloys. Compd.*, 1992, **183**, 413-429.
21. G. M. Sheldrick, *Acta Cryst*. 2008, ***A*** **64**, 112-122.
22. J. C. Scott, S. Etemad, E. M. Engler, *Phys. Rev. B*, 1978, **17**, 2269-2275.
23. A. W. Maverick, J. S. Najdzionek, D. MacKenzie, D. G. Nocera, H. B. Gray, *J. Am. Chem. Soc.*, 1983, **105**,1878-1882.
24. H. Hosoda, Master thesis Kyoto University (2006).
25. T. Mori, A. Kobayashi, Y. Sasaki, H. Kobayashi, G. Saito, H. Inokuchi, *Bull. Chem. Soc. Jpn.*, 1984, **57**, 627-633.
26. H. Kobayashi, H. Tomita, T. Naito, A. Kobayashi, F. Sakai, T. Watanabe, P. Cassoux, *J*. *Am*. *Chem*. *Soc*. 1996, **118**, 368-377.
27. A. Bondi, *J. Phys. Chem*., 1964, **68**, 441–451.
28. a) G. Saito, H. Hosoda, Y. Yoshida, J. Hagiwara, K. Nishimura, H. Yamochi, A. Otsuka, T. Hiramatsu, Y. Shimazaki, K. Kirakci, S. Cordier, C. Perrin, *J. Mater. Chem*., 2012, **22**, 19774-19791.
    b) Y. Yoshida, M. Maesato, Y. Kumagai, M. Mizuno, K. Isomura, H. Kishida, M. Izumi, Y. Kubozono, A. Otsuka, H. Yamochi, G. Saito, K. Kirakci, S. Cordier, C. Perrin, *Eur. J. Inorg. Chem*. 2014, **24**, 3871-3878.
29. a) J. C. Scott, *Mol. Cryst. Liq. Cryst*., 1982, **79**, 49-59.
    b) W. M. Walsh, L. W. Rupp, F. Wudl, M. L. Kaplan, D. E. Schafer, G. A. Thomas, R. Gemmer, *Solid State Commun.*,1980, **33**, 413-416.
30. T. Komatsu, N. Matsukawa, T. Inoue, G. Saito, *J. Phys. Soc. Jpn.*, 1996, **65**, 1340-1354.
31. J. B. Torrance, B. A. Scott, B. Welber, F. B. Kaufman, P. E. Seidenm, *Phys*. *Rev*. *B*, 1979, **19**, 730-741.

Table of contents

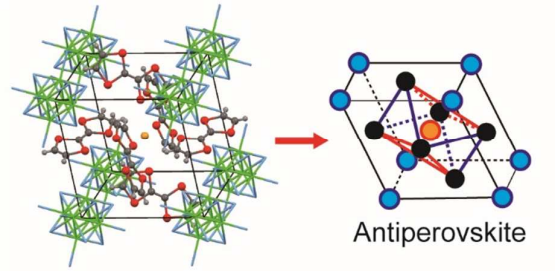

We report two novel antiperovskite charge-transfer solids, $(TSF)_3[(Mo_6X_{14})X]$ (X = Cl, Br), and discuss spin frustration of their octahedral spin lattices.